Advanced Healthcare Materials

ADVANCED HEALTHCARE MATERIALS
www.advhealthmat.de

RESEARCH ARTICLE

Smartphone-Enabled Point-of-Care Biosensing Platform With Self-Calibration for Rapid Matrix-Resistant Detection of Multiple AMI Biomarkers in Whole Blood

Beibei Lu[1,2] | Huaibin Gong[1] | Hua Huang[3] | Kuaifa Fang[4] | Kun Yu[1] | Bitao Lu[1] | Guangqian Lan[1]

[1]State Key Laboratory of Resource Insects, College of Sericulture, Textile and Biomass Sciences, Southwest University, Chongqing, China | [2]College of Pharmaceutical Sciences, Southwest University, Chongqing, China | [3]College of Engineering and Technology, Southwest University, Chongqing, China | [4]Department of Cardiology, The Sixth People's Hospital of Huizhou, Guangdong, China

Correspondence: Guangqian Lan (j070218@swu.edu.cn)

Received: 5 March 2026 | **Revised:** 12 June 2026 | **Accepted:** 19 June 2026

Keywords: acute myocardial infarction | anthraquinone calibration | aptamer | electrochemical biosensor | matrix effect

ABSTRACT

Acute myocardial infarction (AMI) requires rapid diagnosis beyond conventional methods, which suffer from biological interference and complexity, limiting point-of-care (POC) application. To tackle these issues, we have devised an anthraquinone (AQ)-calibrated sensor unit coupled with smartphone-based analysis for universal detection of AMI biomarkers in untreated whole blood. Our novel dual-channel biosensing platform integrates AQ as an intrinsic reference standard, establishing a self-correction mechanism to effectively counteract hematological matrix influences. The platform enables swift quantification at pg/mL levels within 5 min without sample preprocessing, achieving detection limits of 0.3, 19.7, and 0.7 pg/mL for cTnI, Mb, and CK-MB, respectively. The smartphone-based intelligent analyzer automates real-time signal processing, creating a closed-loop POC diagnostic setup that shows promise for future at-home AMI risk monitoring. This technological breakthrough showcases notable resilience to biological matrix interference while upholding analytical sensitivity comparable to clinical standards, representing a significant step toward decentralized cardiovascular emergency management.

1 | Introduction

Cardiovascular diseases (CVDs) remain the leading cause of global mortality [1, 2]. Among CVDs, acute myocardial infarction (AMI) warrants immediate clinical attention due to its disproportionate association with mortality and long-term disability. Epidemiological data from the World Health Organization (WHO) indicate that more than 7 million individuals suffer from AMI each year [3], with mortality patterns showing a significant time-dependent trend [4]. A 10% increase in mortality risk for every 30 min delay in revascularization treatment [5]. This underscores the urgent need for rapid, accurate point-of-care testing (POCT) AMI diagnostic technologies.

Current diagnostic approaches for AMI primarily rely on measuring serum biomarkers such as cardiac troponin I (cTnI), myoglobin (Mb), and creatine kinase-MB (CK-MB) [6, 7]. The selection of these three biomarkers is based on their complementary clinical diagnostic values: cTnI is the gold-standard biomarker with high specificity for myocardial injury; Mb, although less specific, is an early-rising marker critical for initial exclusion; and CK-MB serves as a valuable confirmatory marker for reinfarction monitoring. These biomarkers are released when cardiomyocyte membranes are disrupted and exhibit distinct release patterns that are closely linked to the severity and progression of the infarction [8, 9]. However, widely used analytical methods like chemiluminescence immunoassays (CLIA) [10–12]

and enzyme-linked immunosorbent assays (ELISA) [13–15] have practical limitations. These methods necessitate centralized laboratory facilities, specialized personnel, and strict protocols for isolating plasma/serum, leading to delays of 1–3 h, variability in procedures, and susceptibility to errors before analysis [16–19]. Although emerging point-of-care testing POCT technologies offer promise for decentralized diagnostics [20–22], they are hindered by inherent technical challenges. These limitations include insufficient signal amplification for detecting low-abundance targets, susceptibility to interference from blood components in whole blood samples [23], and involve high production costs—factors that paradoxically impede the portability and affordability required for use in emergency or resource-limited settings [24].

Electrochemical sensing has become a fundamental technology in various fields such as medical diagnostics, environmental monitoring, food safety, and industrial hazard detection due to its unique signal transduction mechanisms [25, 26]. These systems convert specific chemical interactions into measurable electrical outputs (current, potential, or impedance) [27], leading to significant advancements in three key areas [28–30]. First, miniaturization of devices has enabled portable solutions like handheld glucometers and wearable toxin detectors, allowing reagent-free analysis with small sample volumes [31]. Second, sensitivity has been improved through nanomaterial engineering and catalytic signal amplification, achieving detection limits necessary for identifying ultra-trace biomarkers or contaminants. Third, operational reliability has been enhanced by using aptamer (Apt)-based recognition interfaces and advanced antifouling coatings, ensuring consistent performance in diverse media such as whole blood or industrial effluents. The efficiency of modern electrochemical platforms is further demonstrated by their rapid response times, as seen in the detection of the SARS-CoV-2 nucleocapsid protein within 12 min, showcasing their utility in pandemic preparedness [32]. The integration of these nucleic acid receptors into electrochemical biosensing architectures has catalyzed significant progress in biomarker diagnostics by converting selective binding events into quantifiable faradaic responses [33–36]. Illustrative of this capability, screen-printed electrodes (SPEs) engineered with dual-Apt architectures have demonstrated ultrasensitive quantification of cTnI at physiologically critical pg/mL concentrations through optimized amperometric protocols [37, 38]. Nevertheless, operational translation faces persistent barriers arising from hematological matrix complexities. Nonspecific biofouling by plasma proteins (e.g., albumin) and dynamic ionic fluctuations in untreated whole blood induce baseline instability, confounding signal interpretation [39]. Current compensatory approaches, such as including centrifugal plasma isolation or buffer dilution, subvert operational simplicity while introducing preanalytical variability, ultimately contravening the essential "sample-to-answer" paradigm required for emergency diagnostics.

To overcome the limitations inherent in traditional biomarker detection methods, we introduce an innovative hematocompatible biosensing platform that combines AQ-mediated ratiometric electrochemistry with smartphone-based intelligence for versatile AMI diagnosis without the need for pretreatment. This platform utilizes the AQ molecule as an internal reference signal and incorporates a dual-channel self-calibration mechanism to continuously adjust for background interference arising from the complex blood matrix (Scheme 1). By employing this approach, we address the stability issues commonly encountered with conventional single-signal biosensors. The adaptable electrode design allows for the use of different Apt probe configurations, facilitating the universal detection of cTnI, Mb, and CK-MB with a rapid 5 min assay time and sensitivity at the picogram per milliliter level. Moreover, the integration of the intelligent analyzer simplifies signal capture and analytical processing, resulting in a portable closed-loop detection system suitable for self-administered AMI risk assessment by patients. This design replaces simultaneous detection with a universal detection method, which not only avoids the multi-channel crosstalk problem of traditional multi-target POC systems, but also provides higher flexibility and cost efficiency for POC devices. This study presents a clinically applicable solution that balances high sensitivity with operational convenience, promoting a shift towards decentralized and home-based management of CVDs. The proposed technology has the potential to significantly impact pre-hospital AMI diagnosis and enable personalized monitoring of cardiovascular health, thereby facilitating the transition from hospital-based to home-based care in the management of CVDs.

2 | Results and Discussion

2.1 | Characterizations of the AQ-Calibrated Sensor Unit

The assembly process of the AQ-calibrated sensor unit was initially assessed through cyclic voltammetry (CV) and electrochemical impedance spectroscopy (EIS) in a 5 mM $[Fe(CN)_6]^{3-/4-}$ redox probe solution. The kinetics of electron transfer between the redox probe $[Fe(CN)_6]^{3-/4-}$ and the electrode interface are intricately linked to alterations in the electrode surface. Figure 1A,B depicts the CV curves and Nyquist plots (EIS spectra) acquired during the incremental assembly of the AQ-calibrated sensor unit. Upon immobilization of the Apt probe on the bare gold working electrode (AuE), a notable decrease in redox peak currents in the CV curves and a significant increase in semicircle diameter in the EIS spectra were observed. This phenomenon is attributed to the electrostatic repulsion between the negatively charged residues of the Apt probe and the $[Fe(CN)_6]^{3-/4-}$ redox couple in solution, coupled with the steric hindrance introduced by the Apt layer, which further hinders electron transfer at the electrode surface. These effects collectively result in increased impedance and reduced peak currents. Differential Pulse Voltammetry (DPV) was subsequently utilized to analyze variations in the current signal at the electrode surface. As shown in Figure 1C, DPV curves of the AuE in PBS at pH 7.0 were compared before and after Apt probe modification. The AuE did not exhibit any discernible peak currents due to the absence of electroactive species. However, after immobilizing the Apt probe, two distinct reduction peaks were observed at −0.58 and −0.28 V (Figure S3). These peaks were attributed to the presence of electroactive labels AQ and MB, which were conjugated to the Apt probe. AQ exhibits good immobilization stability on the AuE (Figure S9). These electrochemical characterization results validate the successful immobilization of the AQ- and MB-functionalized Apt probe on the AuE surface, thereby confirming the effectiveness of the AQ-calibrated sensor unit fabrication protocol.

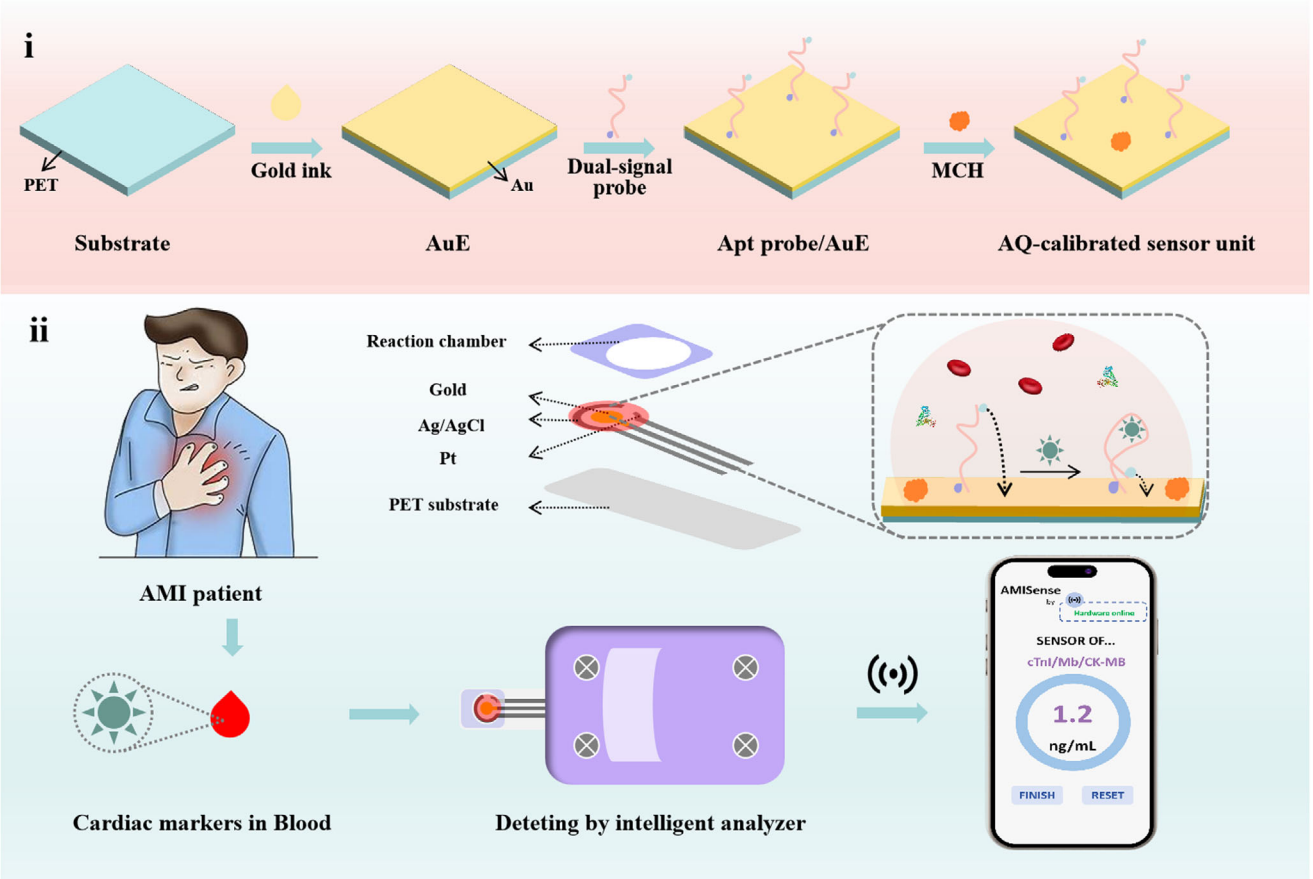

SCHEME 1 | Schematic illustrations of the preparation and detection procedure of the AQ-calibrated sensor unit.

The study examined the wettability of the sensor surface to evaluate the effectiveness of surface modifications by measuring the water contact angle on the gold surface. Contact angle assessments were conducted in this study using a digital camera to evaluate the wettability of the electrodes produced. A droplet of 8 μL of deionized water was placed on the working electrode surface, and the water contact angle was then determined (refer to Figure 1D). The droplet's volume and size remained consistent throughout the experiments. The findings indicated a contact angle of 22.6°on the AQ-calibrated sensor unit surface. A contact angle below 90° signifies a hydrophilic surface. In contrast, the contact angle of the AuE was recorded at 95.9°, confirming its inherent hydrophobic nature. Hydrophobic surfaces readily adsorb proteins and lipids through hydrophobic interactions, leading to biofouling and signal drift. In contrast, hydrophilic surfaces form hydrogen bonds with water molecules, generating a hydration layer that effectively repels hydrophobic biomacromolecules, thereby significantly reducing non-specific adsorption.

The alteration of surface charge throughout the modification process was examined through Zeta potential analysis. Figure 1E illustrates a gradual rise in the electronegativity of the electrode surface following the immobilization of negatively charged Apt probes onto the AuE. This observation unequivocally confirms the effective binding of the Apt probes to the AuE surface. Major blood proteins and cell surfaces are also negatively charged at physiological pH. The increased electronegativity of the electrode surface reduces non-specific adsorption of negatively charged proteins and cells through electrostatic repulsion, thereby lowering background noise and the risk of false positives.

The XPS spectra of the AQ-calibrated sensor unit are depicted in Figure 1F, revealing a distinct Au 4f peak at 84.9 eV, originating from the gold substrate produced by screen-printing Au ink. The P 2p peak (binding energy, BE = 131.2 eV) corresponds to the phosphate groups present within the Apt probe. The S 2p peak (BE = 159.1 eV) confirms the existence of a thiol group (—SH) introduced through the 5'-terminal modification of the Apt probe. Furthermore, the Cl 2p peak (BE = 194.8 eV) is associated with MB molecules conjugated to the Apt probe. These XPS findings collectively establish the successful immobilization of the Apt probe onto the AuE surface. Figure 1G illustrates the elemental mapping images of the sensor unit, demonstrating the presence of Au, S, P, and Cl elements (the electronic image is displayed in Figure S2). The results show that the signals of S (originating from the thiol group), P (from the phosphate backbone of the Apt probe), and Cl (from the MB molecule) are uniformly and continuously distributed across the entire working electrode area (approximately 30 μm × 30 μm), and they overlap well with the Au element signal. This directly demonstrates the excellent uniformity of the Apt probe modification on the electrode surface.

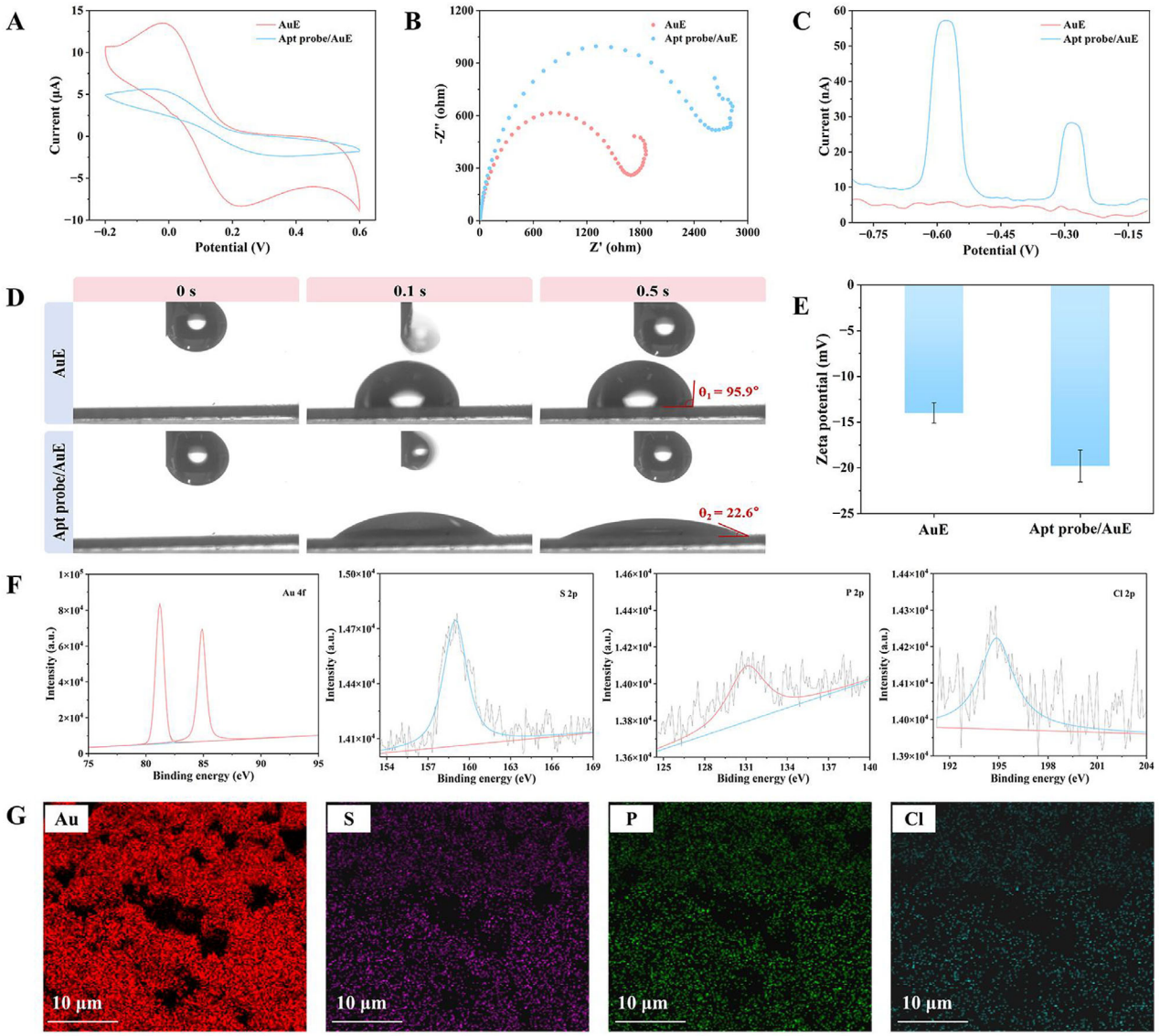

FIGURE 1 | Characterization of the AQ-calibrated sensor unit. CV curves (A) and EIS curves (B) of AuE and Apt probe/AuE in 5 mM $[Fe(CN)_6]^{3-/4-}$ solution, as well as DPV curves (C) in PBS. (D) Water contact angle on the AuE and Apt probe/AuE surface. (E) Zeta potential of AuE and Apt probe/AuE ($n = 3$). Error bars represent standard deviation. (F) XPS spectra of AQ-calibrated sensor unit. (G) The elemental mapping images of the sensor unit, including Au, S, P, and Cl. The scale bar was 10 μm.

2.2 | Selection and Validation of Apt Probe Sequences

The Apt targeting cTnI, Mb, and CK-MB were chosen based on prior studies. The recognition and binding interactions between the three Apt and their targets were assessed using circular dichroism (CD) spectroscopy (Figure 2A–C). The CD spectra of the isolated targets (cTnI, Mb, CK-MB) did not exhibit distinct absorption peaks. In contrast, the unbound Apt showed characteristic negative and positive peaks around 245 and 275 nm, respectively. Upon incubation and binding of the Apt with its targets, the peak amplitudes decreased significantly due to structural changes in the Apt's helical conformation, particularly in base stacking interactions. Importantly, the peak positions remained mostly unchanged. The decrease in peak amplitude induced by binding confirmed the specific interactions between cTnI, Mb, and CK-MB and their respective Apt. These findings affirm the appropriateness of the selected Apt sequences for subsequent analytical purposes, thus endorsing the effectiveness of the proposed detection approach.

2.3 | Evaluation of Calibration Performance Using AQ as an Internal Reference

To assess the calibration performance of the electroactive label AQ during blood sample detection, we compared the response of cTnI sensor units with and without AQ to varying cTnI concentrations in whole blood (Figure 2D,E). The normalized current change (I_{Nor}) was calculated using the following equations:

$$R = \frac{I_{MB}}{I_{MB0}} - \frac{I_{AQ}}{I_{AQ0}} \quad (1)$$

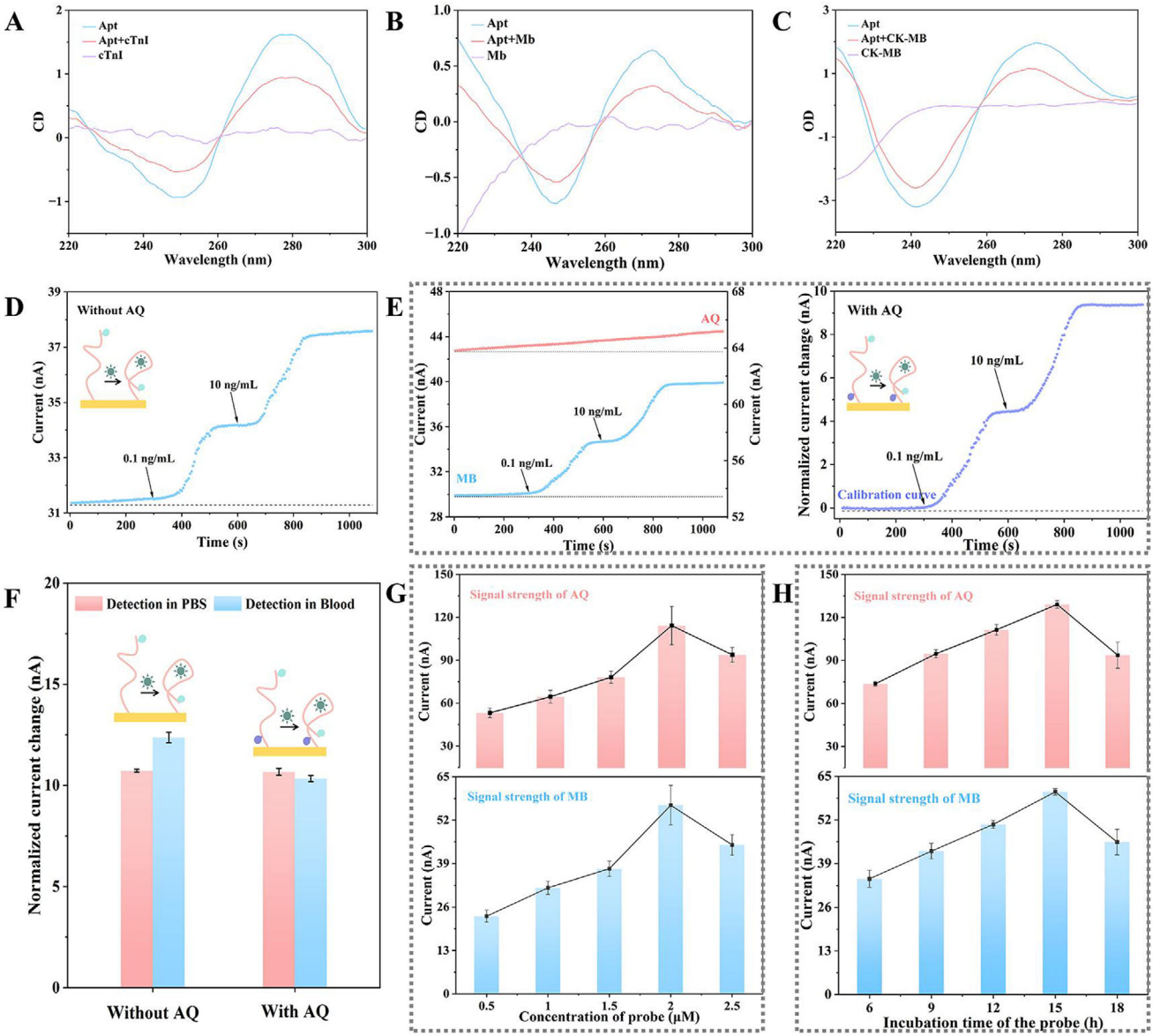

FIGURE 2 | Sensing feasibility and performance of the AQ-calibrated sensor unit. The CD spectra of the cTnI (A), Mb (B), and CK-MB (C) to Apt probe. (D) Amperometric i-t curves of AQ-free sensor unit in whole blood. (E) Amperometric i-t curves and normalized current curves of AQ-calibrated sensor unit in whole blood. (F) Comparison of the response of the sensor unit to cTnI in the presence and absence of AQ. Changes in current intensity of the AQ-calibrated sensor unit at different Apt probe concentrations (G) and incubation times (H) ($n = 3$). Error bars represent standard deviation.

$$I_{Nor} = R \times I_{MB0} \quad (2)$$

where I_{MB0} and I_{AQ0} represent the initial currents of MB and AQ in the absence of the target, respectively, while I_{MB} and I_{AQ} denote the final currents after target binding. For sensor units without AQ, I_{AQ0} and I_{AQ} are zero. The parameter R (Rate) reflects the relative change in electrochemical signals during detection, and I_{Nor} quantifies the calibrated MB current relative to AQ. Notably, the I_{Nor} of AQ-calibrated sensor unit approached zero after 300 s of baseline drift in blood, demonstrating effective drift correction.

Upon exposure to cTnI-spiked blood samples, the sensor unit calibrated with AQ effectively mitigated baseline drift (Figure S4). This was confirmed by comparing the responses of AQ-free and AQ-calibrated sensor units across various concentrations of cTnI over a 780 s period. In the absence of AQ, the MB signal displayed a continuous upward drift, leading to baseline tilting and overestimation of currents (Figure 2D). In contrast, the AQ-calibrated sensor unit maintained a stable baseline with minimal drift (Figure 2E), highlighting the superior and consistent calibration performance of AQ in complex blood matrices. Additionally, the AQ-calibrated sensor unit achieved a steady state within 5 min of exposure to cTnI (Figure 2E), validating its rapid kinetics (Table S2 and Figure S7) and suitability for rapid detection (≤ 5 min).

To assess target response performance, sensor units were fabricated using AQ-modified and AQ-free Apt probes and tested in PBS and blood samples. The left panel of Figure 2F (inset) demonstrates the utilization of the AQ-free sensor unit as a negative control. A notable disparity in target response between PBS and blood matrices was observed when comparing the AQ-free sensor unit to the AQ-calibrated sensor unit. This finding

underscores the enhanced accuracy of the AQ-calibrated sensor unit in detecting blood samples, attributed to the AQ electroactive label's effective baseline drift correction capability.

2.4 | Optimization of AQ-Calibrated Sensor Unit Performance Parameters

To optimize the detection performance of the AQ-calibrated sensor unit, crucial parameters affecting analytical efficacy, such as Apt probe concentration and incubation time, were methodically fine-tuned before formal testing. As depicted in Figure 2G, the peak currents of AQ and MB exhibited an increase with Apt probe concentration ranging from 0.5 to 2 μM, indicating heightened electrochemical activity attributed to increased probe loading. The most robust response signal was observed at 2 μM. However, elevating the concentration to 2.5 μM resulted in diminished peak currents, likely due to steric hindrance impeding electrochemical accessibility at the electrode surface. Therefore, 2 μM was determined as the optimal Apt probe concentration for subsequent experiments. Figure 2H demonstrates the impact of incubation time (6, 9, 12, 15, and 18 h) on Apt probe immobilization on the AuE surface. Prolonged incubation exceeding 15 h led to decreased probe activity, possibly as a result of denaturation or nonspecific adsorption. Consequently, 15 h was established as the optimal incubation duration to strike a balance between probe density and functional integrity.

2.5 | Detection Performance of the AQ-Calibrated Sensor Unit

To validate the detection capabilities of the AQ-calibrated sensor unit, we utilized it for the diagnosis of AMI. cTnI, Mb, and CK-MB are established biomarkers that exhibit alterations during AMI, indicative of pathological conditions in individuals. Conventional biosensing approaches typically operate in simplistic matrices, such as PBS or serum, which often fall short in mitigating the presence of interfering substances in blood samples, consequently compromising reliability and precision. In contrast, the AQ-calibrated sensor unit presents a dependable means for the direct detection of AMI biomarkers in whole blood, offering a promising avenue for the prompt diagnosis of AMI. Through meticulous optimization, we assessed the sensing efficacy of the AQ-calibrated sensor unit by examining its response to varying concentrations of the target analytes (cTnI, Mb, CK-MB) in both PBS (refer to Figure S5) and blood matrices (refer to Figure S6). As shown in Figure 3A,B, the normalized current change (I_{Nor}) exhibited a concentration-dependent increase for all targets (cTnI, Mb, CK-MB) in both PBS and blood, with strong linear correlations between I_{Nor} and the logarithm of target concentrations. The detection standard curves of the AQ-calibrated sensor unit in PBS are $y_{(cTnI)} = 9.01327+2.29204x$ ($R^2 = 0.9952$), $y_{(Mb)} = 11.53824+4.68431x$ ($R^2 = 0.9940$), and $y_{(CK\text{-}MB)} = 13.57086+4.05485x$ ($R^2 = 0.9989$). The detection standard curves in Blood are $y'_{(cTnI)} = 8.31447+2.28329x'$ ($R^2 = 0.9978$), $y'_{(Mb)} = 9.51212+5.57444x'$ ($R^2 = 0.9921$), and $y'_{(CK\text{-}MB)} = 10.78658+3.38388x'$ ($R^2 = 0.9990$), where y is I_{Nor} and x is the logarithm of the target concentration.

A direct comparison of responses in PBS and blood matrices (Figure 3C) revealed nearly identical I_{Nor} values for equivalent target concentrations (cTnI, Mb, CK-MB). This confirms that the AQ-calibrated sensor unit retains excellent detection fidelity in complex blood environments, with acceptable detection limits (LOD) and dynamic detection ranges (cTnI, 0.3 pg/mL, 10 pg/mL—500 ng/mL. Mb, 19.7 pg/mL, 100 pg/mL—1000 ng/mL. CK-MB, 0.7 pg/mL, 10 pg/mL—500 ng/mL). While the detection sensitivity in blood samples is higher than in the PBS matrix (cTnI, 0.12 pg/mL, 1 pg/mL—500 ng/mL. Mb, 3.49 pg/mL, 10 pg/mL—1000 ng/mL. CK-MB, 0.46 pg/mL, 1 pg/mL—500 ng/mL), the observed detection range aligns with variations in cardiac muscle markers in the PBS sample and remains below the detection range of normal cardiac muscle marker levels. Consequently, we introduce a functional nano-biosensing platform capable of precise and sensitive AMI diagnosis. The LODs are far below the clinical diagnostic cutoffs for AMI. Moreover, the linear ranges fully cover the clinically relevant concentration intervals, from normal baseline to highly elevated AMI levels [40–42]. This exceptional sensitivity and wide dynamic range, combined with direct whole-blood compatibility, make our platform highly promising for rapid and accurate POC diagnosis of AMI.

2.6 | Specificity, Versatility, Reproducibility, and Stability of the AQ-Calibrated Sensor Unit

Control experiments were conducted to evaluate the specificity of the AQ-calibrated sensor unit by testing common post-myocardial infarction biomarkers as interferents, including cTnI, Mb, CK-MB, heart-type fatty acid-binding protein (H-FABP), C-reactive protein (CRP), skeletal troponin I (sTnI), hemoglobin (Hb), muscle-type CK (CK-MM), and brain-type CK (CK-BB). Interferents were present at a concentration of 100 ng/mL, while targets were at 10 ng/mL, resulting in an interferent-to-target ratio of 10:1. The electrochemical signal of the AQ-calibrated sensor unit, as depicted in Figure 4A, remained unchanged in the presence of interferents but exhibited a significant response upon the introduction of cTnI. This observation confirms the sensor unit's exceptional specificity against interference in blood matrices. To showcase its versatility, the cTnI-specific Apt probe was substituted with Mb- and CK-MB-specific Apt probes to detect Mb and CK-MB, respectively. Figure 4B,C demonstrate that the AQ-calibrated sensor unit maintained comparable specificity and sensitivity for these alternative targets. Through the modular exchange of Apt probes, the system can be tailored to detect multiple analytes, underscoring its wide-ranging utility in multiplex biomarker detection.

High repeatability and stability are crucial characteristics of the AQ-calibrated sensor unit. Following a 30-min incubation period, the sensor unit can be effectively regenerated under acidic conditions (pH 5.0) for repetitive target quantification (Figure 4D). Using cTnI as a model analyte, the AQ-calibrated sensor unit exhibited an 89.6% recovery rate for cTnI detection after four regeneration and measurement cycles, underscoring its dependable repeatability (Figure 4E). Moreover, the AQ-calibrated sensor unit exhibits good stability, reversibility, and excellent preparation reproducibility (Figure S10). To assess long-term stability, the sensor unit was evaluated in blood samples spiked with 10 ng/mL cTnI, Mb and CK-MB and stored at 25°C. Measurements were conducted every 7 days over a period of 28 days. As depicted in Figure 4F, the electrochemical

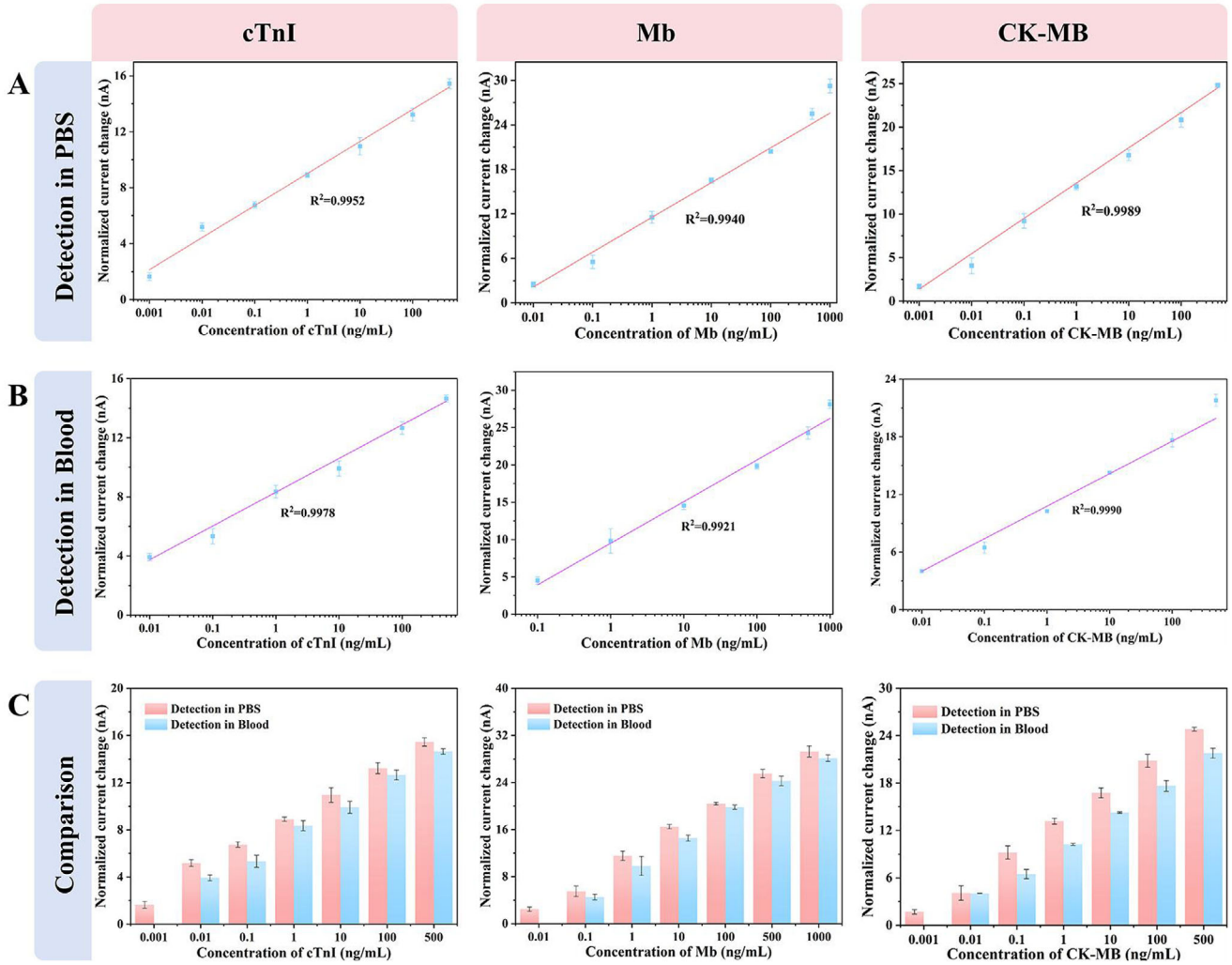

FIGURE 3 | Results of the response of the AQ-calibrated sensor unit to cTnI, Mb, and CK-MB. (A) Linear relationship between the I_{Nor} and the concentration of target in PBS. (B) Linear relationship between the I_{Nor} and the concentration of the target in blood. (C) The comparison of target responses at different concentrations of cTnI, Mb, and CK-MB in PBS blood ($n = 3$). Error bars represent standard deviation.

signal response to all three AMI biomarkers (cTnI, Mb, and CK-MB) remained largely consistent over a 28-day duration, indicating satisfactory operational stability for AMI biomarker detection applications. Furthermore, the detection performance under different environmental conditions (Figure S8) confirmed the intrinsic stability of the self-calibration mechanism itself.

2.7 | Design of the Intelligent Analyzer

The biosensing platform has been successfully developed, consisting of three main modules: an AQ-calibrated sensor unit and an intelligent analyzer (a printed circuit board (PCB) and a smartphone equipped with a dedicated app) (Figure S11). The biosensing platform architecture, illustrated in Figure 5A, follows a hierarchical design flow starting from the AQ-calibrated sensor unit to the PCB assembly, culminating in integration with a dedicated smartphone application. The PCB is equipped with a Bluetooth interface to wirelessly transmit captured electrical signals to the smartphone. Subsequently, these signals undergo digital processing and are displayed through the application interface. Developed using Altium Designer 16.1.12, the PCB features a potentiostat circuit configuration, serving as the core functional component of an intelligent analyzer. Figure 5B displays the technical schematics of the PCB, showcasing multilayer routing diagrams for both the top and bottom layers, along with 2D and 3D computer-aided design (CAD) renderings. The biosensing platform enables universal detection of different AMI biomarkers by exchanging the Apt probe-modified sensor unit. Each measurement targets a single biomarker, thus avoiding signal cross-talk.

2.8 | Real Sample Analysis and Method Comparison

A linear regression analysis curve was created to assess the performance of the intelligent analyzer by comparing the measured values from the analyzer with the actual target concentrations (the demonstration video of the detection process of the intelligent analyzer can be found in Videos S1–S4). The analysis revealed high correlation coefficients (R^2) of 0.9991, 0.9995, and 0.9994 for cTnI, Mb, and CK-MB, respectively (Figure 5C).

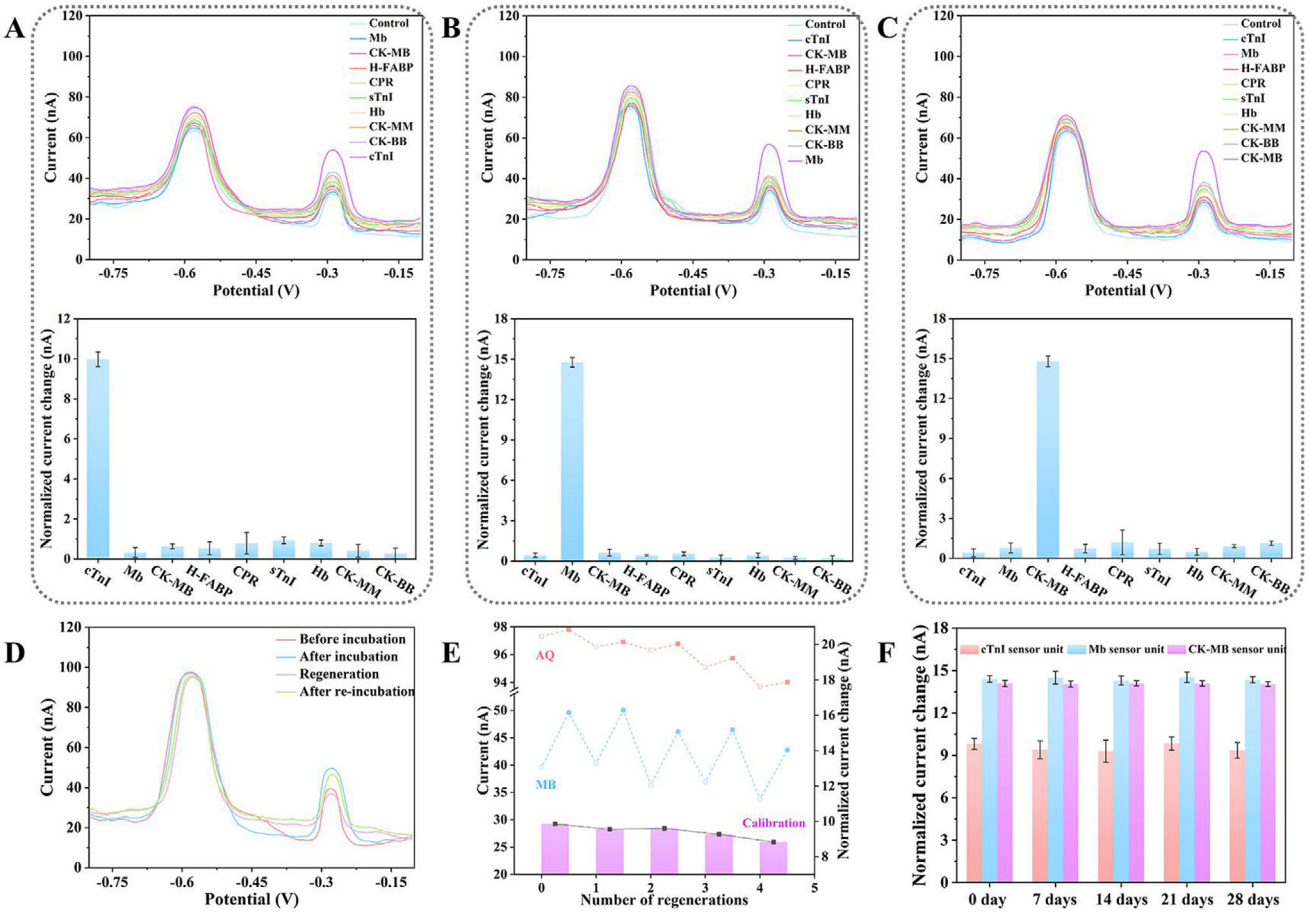

FIGURE 4 | Performance evaluation of the AQ-calibrated sensor unit. (A–C) Specificity and universality evaluation of the AQ-calibrated sensor unit in blood matrices. The DPV curves (D) and the corresponding peak current (E) show the regeneration and repetitive use of the AQ-calibrated sensor unit with 10 ng/mL of cTnI under acidic conditions (pH 5.0). (F) I_{Nor} change of the AQ-calibrated sensor unit with 10 ng/mL of cTnI, Mb, and CK-MB at 25°C ($n = 3$). Error bars represent standard deviation.

These findings confirm the accuracy and reliability of the intelligent analyzer as a portable detection platform for AMI biomarkers.

A thorough comparative analysis was conducted utilizing ELISA kits, the CHI660E electrochemical workstation, and an intelligent analyzer to evaluate blank samples and blood specimens spiked with cTnI, Mb, and CK-MB. Figure 5D depicts the calibration curves generated from the cTnI, Mb, and CK-MB ELISA kits, demonstrating R^2 of 0.9904, 0.9919, and 0.9961, respectively. Tabulated comparative findings are presented in Table 1. The results unequivocally establish the superior performance of the intelligent analyzer and CHI660E electrochemical workstation over ELISA kits in terms of sensitivity, accuracy, detection range, and operational procedures. Moreover, a comprehensive comparison of the platform with previously reported methods for AMI biomarker detection (Table S3) and with existing drift correction strategies (Table S4) is provided in the Supporting Information, highlighting the advantages of our AQ-calibrated self-correction mechanism in terms of detection range, assay time, matrix tolerance, and system simplicity.

Besides, we have verified the analytical performance of the analyzer on clinical specimens. In brief, we have performed a blind analysis of the three AMI biomarkers (cTnI, Mb, and CK-MB) using whole blood samples from 5 AMI patients (Patient Group, PG) and 5 healthy volunteers (Healthy Group, HG). The collection and testing of patient blood samples were approved by the Medical Ethics Committee of Huizhou Sixth People's Hospital (Approval No. KYYJ2025-LY066). This approval was valid for the entire duration of the study, from sample collection to data analysis. Informed consent was obtained from all individual participants (including both AMI patients and healthy volunteers) involved in the study. The detection results demonstrated that the measured concentrations of all three AMI biomarkers in the PG were significantly higher than those in the HG (Figure 5E). Furthermore, statistical analysis (using a t-test) revealed significant differences between the PG and HG groups (**, $p < 0.01$), with Cohen's d effect sizes of 2.73 for cTnI, 2.52 for Mb, and 2.49 for CK-MB, indicating the potential clinical utility of the platform. However, the clinical validation was performed with a small sample size (5 AMI patients and 5 healthy volunteers). While the large effect sizes and significant differences support the proof-of-concept of this platform, the results should not be generalized to the broader AMI population. Future multi-center studies with substantially larger cohorts are required to determine diagnostic cut-offs, sensitivity, and real-world performance.

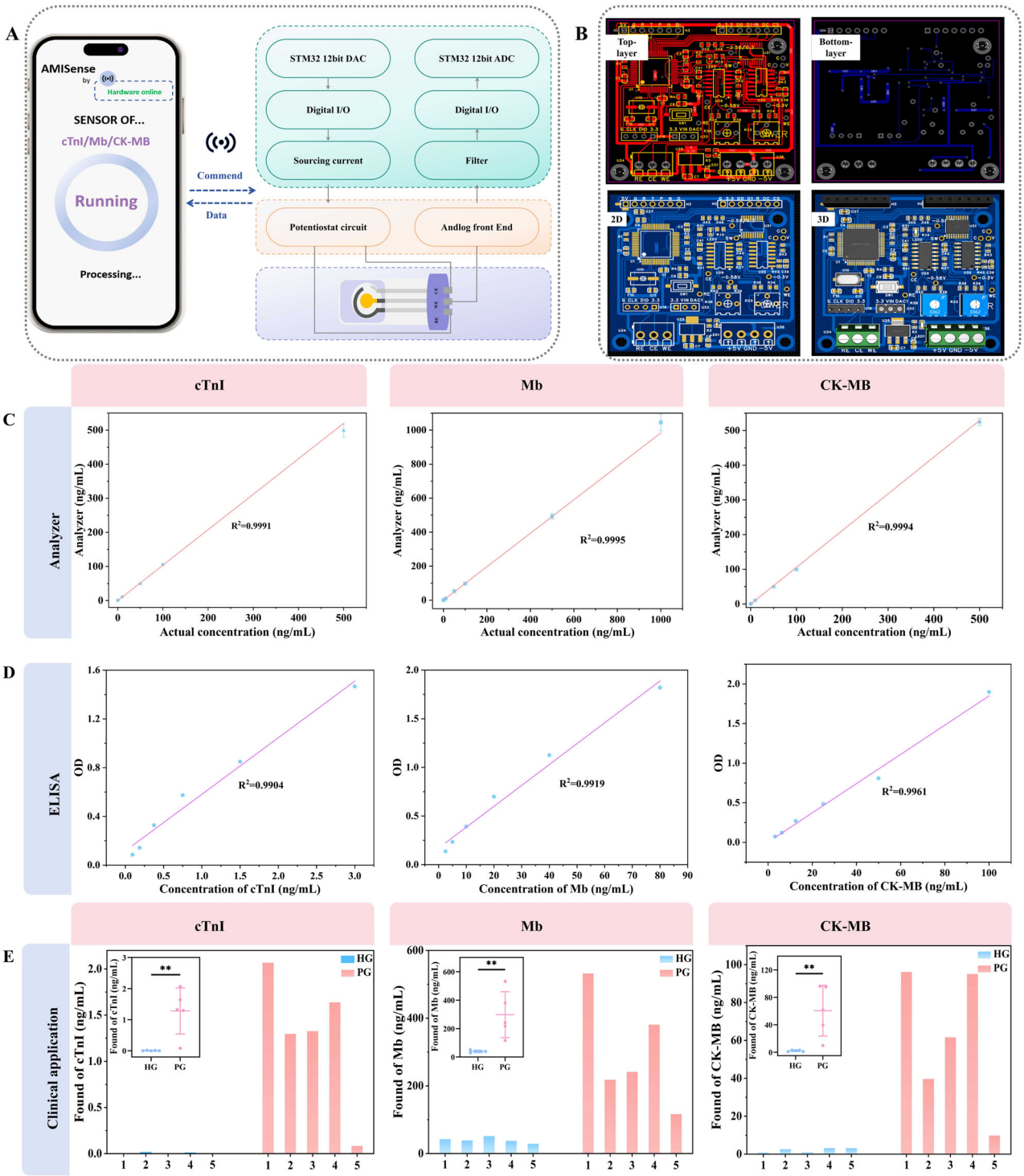

FIGURE 5 | Design of the intelligent analyzer and Analysis of Accuracy. (A) Schematic diagram of the intelligent analyzer. (B) Wiring diagram of the PCB. (C) Linear regression analysis of the intelligent analyzer against actual target concentrations of cTnI, Mb, and CK-MB. (D) Calibration curves derived from ELISA kits of cTnI, Mb, and CK-MB. (E) Measured concentration of the clinical specimens collected from HG ($n = 5$) and PG ($n = 5$). The insets are scatterplots of the clinical specimens of HG and PG. Statistical significance was determined by a two-tailed unpaired Student's *t*-test (**, $p <$ 0.01).

3 | Conclusion

This study developed a biosensing platform compatible with whole blood for detecting myocardial biomarkers. The platform is based on AQ-calibrated electrodes and was integrated with a smartphone terminal to create a POCT biosensing platform. By utilizing AQ molecules as calibration signals, a dual-channel self-calibration model was established, reducing the relative standard deviation of whole blood detection from 8.2% (using conventional methods) to 3.1%. This significantly improved

TABLE 1 | Recovery experiment for the detection of different concentrations of target in whole blood samples.

		Analyzer		CHI660E		ELISA kit	
Sample	Spiker (ng/mL)	Found (ng/mL)	Recovery (%)	Found (ng/mL)	Recovery (%)	Found (ng/mL)	Recovery (%)
cTnI	0	Nd		Nd		Nd	
	0.1	0.109	109.3 ± 4.16	0.102	101.7 ± 2.48	0.113	112.9 ± 8.71
	1	0.984	98.4 ± 3.12	0.998	99.83 ± 3.07	0.948	94.8 ± 7.69
	50	49.339	98.7 ± 3.15	51.244	102.5 ± 5.90	Nd	
Mb	0	Nd		Nd		Nd	
	0.1	0.101	101.3 ± 3.79	0.108	107.7 ± 3.26	Nd	
	1	1.028	102.8 ± 3.76	0.9255	92.55 ± 3.58	Nd	
	50	52.900	105.8 ± 2.44	53.097	106.2 ± 2.48	45.44	90.88 ± 8.81
CK-MB	0	Nd		Nd		Nd	
	0.1	0.111	111.3 ± 2.52	0.095	95.13 ± 3.60	Nd	
	1	1.059	105.9 ± 1.77	1.071	107.1 ± 2.16	Nd	
	50	49.715	99.4 ± 3.22	52.893	105.8 ± 3.17	48.589	97.18 ± 7.73

Abbreviation: Nd, not detected.

Recovery (%) is expressed as mean ± SD. $n = 3$, each spiked concentration was obtained from three parallel experiments.

detection reliability in complex matrices. Additionally, the Apt-functionalized electrode technology allowed for the universal detection of cardiac biomarkers (cTnI, Mb, and CK-MB) with sensitivities in the picogram per milliliter range, meeting clinical diagnostic thresholds. The biosensing platform was designed with coordinated hardware-software integration, incorporating smartphone Bluetooth modules and a customized mini-program. This design enabled wireless electrochemical signal acquisition, real-time analysis, and cloud-based report generation. Its power consumption was maintained below 10 mW, and the cost per test was under $2. Experimental validation confirmed the sensor's high consistency with reference results in whole blood samples ($R^2 > 0.999$) and demonstrated stability for at least 28 days under ambient conditions (25°C). This research supports the feasibility of pre-hospital early detection of AMI using a low-cost, portable platform. The design framework is versatile and could potentially be expanded to monitor other disease biomarkers at home.

4 | Experimental Section

4.1 | Materials and Reagents

Tris-(2-carboxyethyl)-phosphine hydrochloride (TCEP) and cardiac troponin I (cTnI) were purchased from Sigma-Aldrich Co. (St. Louis, MO, USA). 6-mercapto-1-hexanol (MCH) and myoglobin (Mb) were obtained from Aladdin. Creatine kinase-MB (CK-MB) was purchased from Prospec Ltd., Israel. Heart-type fatty acid-binding protein (H-FABP) and C-reactive protein (CRP) were purchased from Abcam Trading Co., Ltd., Shanghai, China. Creatine kinase-MM (CK-MM) and creatine kinase-BB (CK-BB) were purchased from Shanghai Xibao Biotechnology Co., Ltd. PBS phosphate buffer and anhydrous ethanol were purchased from Beijing Solarbio Science & Technology Co., Ltd. ELISA kits for cTnI, Mb, and CK-MB of humans were purchased from Jiangsu Meimian Industrial Co., Ltd. (MEIMIAN, Jiangsu, China). SPEs (Figure S1) (12 × 34 mm^2, 2 mm diameter disk working electrode, gold powder working electrode, platinum powder counter electrode, Ag/AgCl pellet reference electrode) were purchased from Poten Technology Co., Ltd. (Weihai, China). And all oligonucleotide sequences purified by HPLC were synthesized by Integrated DNA Technologies, confirmed by HPLC profile and mass spectrometry. The sequences used in this study are listed in Table S1. All solvents and chemicals were analytical reagents and were used without further purification.

4.2 | AQ-Calibrated Sensor Unit Fabrication

Before assembly, the SPEs were sequentially rinsed three times with ethanol and deionized water to remove residual organic contaminants and oxide layers from the printing process, ensuring precise and reliable detection outcomes. The cleaned SPEs were air-dried on a sterile bench for subsequent processing. All thiol-modified oligonucleotide Apt probes were reconstituted in phosphate-buffered saline (PBS, pH 7.0) to a final concentration of 100 μM, aliquoted, and stored at -20°C until use.

For the fabrication of the AQ-calibrated sensor unit, the Apt probe solution was mixed with an equal volume of 1 mM TCEP solution and incubated at room temperature for 1 h. TCEP reduces disulfide bonds to free thiols (—SH) while maintaining the structural integrity of the Apt probes. Subsequently, 10 μL of the reduced Apt-TCEP mixture was dropped onto the freshly cleaned working electrode surface of the SPE. The modified electrode was incubated at 4°C for a defined duration to facilitate Apt immobilization. Optimal assembly conditions were established by systematically varying Apt concentrations and immobilization times. Post-immobilization, the AQ-calibrated sensor unit was rinsed with deionized water and passivated with 1 mM MCH solution for 1 h at ambient temperature to displace nonspecifically adsorbed Apts and block residual binding sites.

Before electrochemical characterization, the functionalized AQ-calibrated sensor unit was rigorously washed with deionized water to remove unbound reagents.

4.3 | Characterization Techniques

The surface chemical composition was characterized using a multifunctional x-ray photoelectron spectrometer (XPS), specifically the AXIS SUPRA+ system (Shimadzu Co., Japan) equipped with a monochromatic Al Kα x-ray source (1486.6 eV). Zeta potential measurements were performed using an electrokinetic solid surface analyzer: SurPASS 3 (Anton Paar GmbH, Austria) under controlled electrolyte conditions. Circular dichroism (CD) spectra were acquired on a Chirascan V100 Circular Dichroism Spectrometer (Applied Photophysics Ltd, UK) with a quartz cuvette of 1 mm path length. Static contact angles were determined using a DSA100 fully automated single-fiber contact angle goniometer (KRÜSS GmbH, Germany) under ambient conditions. All electrochemical experiments were conducted at room temperature using a CHI660E electrochemical workstation (CH Instruments, Shanghai, China). Differential Pulse Voltammetry (DPV): Performed with a potential window of −0.1 to −0.8 V, amplitude of 0.05 V, and pulse width of 0.025 s. Amperometric i-t curves: Current data were recorded at 5 s intervals under a constant applied potential.

4.4 | Design of the Intelligent Analyzer

The intelligent analyzer consists of three core components: a signal acquisition printed circuit board (PCB), a smartphone integrated with a dedicated mini-program, and an AQ-calibrated sensor unit. The schematic diagram of the PCB signal acquisition circuit board is illustrated in Figure S12. Chemical signals derived from the sensor unit are transduced into measurable electrical signals and digitized via a 12-bit analog-to-digital converter (ADC) embedded within the microcontroller unit (MCU). Bidirectional communication between the analyzer and the smartphone is established through a 4G wireless module (Figure S13). The smartphone transmits detection commands to the analyzer via the 4G network, while the custom-developed mini-program enables remote control of the analyzer, real-time data acquisition, signal processing, and visualization of results on the smartphone interface. The reliability of the system for practical detection was validated by cross-comparison of analytical results obtained from the smart analyzer, CHI660E electrochemical workstation, and ELISA.

4.5 | Preparation and Testing of the Target Concentration in Actual Blood Samples

The evaluation of target analytes in human blood samples in this study adhered to the ethical guidelines approved by the Life and Medical Ethics Committee of Southwest University. Fresh blood samples were collected using vacuum phlebotomy needles into EDTA anticoagulant tubes, gently mixed, and immediately stored at 4°C. The target protein was removed by immunoaffinity depletion prior to use.

The quantification of the target in blood samples was conducted through ELISA using a BioTek Epoch microplate spectrophotometer (Agilent Technologies, USA) with absorbance readings at 450 nm. For the analysis of the target in blood samples, such as cTnI, a smartphone-based intelligent analyzer test was employed. The operational steps are as follows: 1. Device Initialization: Access the mini-program interface, connect to the analyzer, and choose the target analyte (e.g., “cTnI”). 2. Sample Application: When prompted with “Drop your sample” on the screen, apply 40 μL of the blood sample onto the sensor unit’s surface. 3. Automated Detection: Press the “OK” button immediately to commence the test. The concentration of measured cTnI is presented on the smartphone interface after a 5-min incubation period. Post-testing, discrepancies between the results obtained from the Intelligent analyzer, CHI660E electrochemical workstation, and ELISA were calculated and recorded to validate the analytical consistency and reliability of the integrated system.

4.6 | Ethics Statement

The evaluation of target analytes in healthy human blood samples in this study adhered to the ethical guidelines approved by the Life and Medical Ethics Committee of Southwest University (SWU-ETH-2025-04-24-001). The collection and testing of patient blood samples were approved by the Medical Ethics Committee of Huizhou Sixth People’s Hospital (Approval No. KYYJ2025-LY066). The approvals were valid for the entire duration of the study, from sample collection to data analysis. Informed consent was obtained from all individual participants (including both AMI patients and healthy volunteers) involved in the study.

4.7 | Statistical Analysis

All electrochemical measurements were performed using independent AQ-calibrated sensor units. Unless otherwise stated, each experimental condition was repeated using three independently fabricated sensor units. For calibration curves, each concentration point was measured using three independent sensor units. The number of replicates (n) is indicated in each figure caption. Quantitative data are presented as mean ± SD. For comparisons between two groups (AMI patient group vs. healthy control group), a two-tailed unpaired Student’s *t*-test was performed. The significance level (α) was set at 0.05. In all cases, a p-value < 0.05 was considered statistically significant. All data were processed and analyzed using OriginPro 2025 (OriginLab Corporation, USA).

Author Contributions

Beibei Lu: conceptualization, data curation, formal analysis, investigation, methodology, validation, visualization, writing – original draft, writing – review and editing. **Huaibin Gong**: investigation, methodology. **Hua Huang**: methodology, validation. **Kuaifa Fang**: investigation, methodology. **Kun Yu**: writing – review and editing. **Bitao Lu**: investigation, methodology. **Guangqian Lan**: conceptualization, data curation, formal analysis, writing – review and editing, funding acquisition, project

administration, resources, supervision. The manuscript was written through the contributions of all authors. All authors have given approval to the final version of the manuscript.

Funding

This study was supported by the Sichuan Science and Technology Program (No. 2024ZYD0177), the Natural Science Foundation of Chongqing, China (No. CSTB2024NSCQ-LZX0018), and the Natural Science Foundation of Chongqing, China (No. cstc2021jcyj-cxtt0005).

Conflicts of Interest

The authors declare no conflicts of interest.

Data Availability Statement

The data that support the findings of this study are available from the corresponding author upon reasonable request.

References

1. A. G. M. Brown, S. Adas, J. de Jesus, N. Farmer, R. Fisher, and C. A. Pratt, "Bridging the Gap: The Need to Implement Dietary Guidance to Address Cardiovascular Health," *Nutrients* 16, no. 13 (2024): 2125, https://doi.org/10.3390/nu16132125.

2. B. G. Olutola, N. S. Mwase, J. Shirinde, and J. Wichmann, "Apparent Temperature Modifies the Effects of Air Pollution on Cardiovascular Disease Mortality in Cape Town, South Africa," *Climate* 11, no. 2 (2023): 30.

3. W. H. Ge, Y. Lin, S. Li, X. Zong, and Z. C. Ge, "Identification of Biomarkers for Early Diagnosis of Acute Myocardial Infarction," *Journal of Cellular Biochemistry* 119, no. 1 (2017): 650–658, https://doi.org/10.1002/jcb.26226.

4. Y. Liu, W. Li, S. An, et al., "Relationship Between 24 h Blood Pressure Variability and Mortality in Acute Myocardial Infarction Patients," *Clinical Cardiology* 47, no. 4 (2024): 24261, https://doi.org/10.1002/clc.24261.

5. J. Park, K. H. Choi, J. M. Lee, et al., "Prognostic Implications of Door-to-Balloon Time and Onset-to-Door Time on Mortality in Patients With ST-Segment–Elevation Myocardial Infarction Treated With Primary Percutaneous Coronary Intervention," *Journal of the American Heart Association* 8, no. 9 (2019): 012188, https://doi.org/10.1161/JAHA.119.012188.

6. M. L. Castillo, A. Acena, A. M. Pello-Lazaro, et al., "Prognostic Value of Initial QRS Analysis in Acute Anterior Myocardial Infarction: Correlation With Left Ventricular Systolic Dysfunction, Serum Biomarkers, and Cardiac Outcomes," *European Heart Journal* 26, no. 1 (2020): 12791.

7. X. L. Yue, X. Y. Shi, M. Jiang, and R. J. Li, "Acute Pulmonary Embolism Presenting With Electrocardiographic Signs and Serum Biomarkers of ST-Segment Elevation Myocardial Infarction: A Case Report," *Journal of International Medical Research* 51, no. 9 (2023): 3000605231197063, https://doi.org/10.1177/03000605231197063.

8. J. Egan, J. Skowno, D. T. M. Le, C. T. Goh, M. S. Festa, and D. Winlaw, "Markers of Myocardial Injury Study," *Australian Critical Care* 33, no. 1 (2020): S8–S9, https://doi.org/10.1016/j.aucc.2020.04.025.

9. J. Neumann, N. A. Soerensen, T. S. Hartikainen, et al., "Discrimination of Myocardial Infarction and Myocardial Injury Using a Multibiomarker Approach," *European Heart Journal* 113, no. 12 (2020): 1682–1691.

10. G. R. Han, A. Goncharov, M. Eryilmaz, et al., "Deep Learning-Enhanced Chemiluminescence Vertical Flow Assay for High-Sensitivity Cardiac Troponin I Testing," *Small* 21, no. 11 (2025): 2411585.

11. C. Hong, P. Zhang, K. Lu, et al., "A Dual-Signal Electrochemiluminescence Immunosensor for High-Sensitivity Detection of Acute Myocardial Infarction Bio Marker," *Biosensors and Bioelectronics* 194 (2021): 113591, https://doi.org/10.1016/j.bios.2021.113591.

12. S. Mansouri, S. Oudah Mezan, F. M. A. Altalbawy, et al., "Recent Advances in Assembly Strategies of New Advanced Materials-Based Analytical Methods for the Detection of Cardiac Biomarkers as a Diagnosis Tool," *Microchemical Journal* 191 (2023): 108827, https://doi.org/10.1016/j.microc.2023.108827.

13. Y. He, X. Gu, Y. Hu, et al., "Low-Density Lipoprotein Receptor and Apolipoprotein A 5, Myocardial Infarction Biomarkers in Plasma-Derived Exosomes," *Journal of Cardiology* 79, no. 5 (2022): 605–610, https://doi.org/10.1016/j.jjcc.2021.10.020.

14. L. Hu, M. Rossetti, J. F. Bergua, et al., "Harnessing Bioluminescent Bacteria to Develop an Enzymatic-Free Enzyme-Linked Immunosorbent Assay for the Detection of Clinically Relevant Biomarkers," *ACS Applied Materials & Interfaces* 16, no. 24 (2024): 30636–30647, https://doi.org/10.1021/acsami.4c01744.

15. J. Zheng, Y. Qiu, Y. Xu, et al., "Magnetic Particle-Based Chemiluminescence Immunoassay for Serum Human Heart-Type Fatty Acid Binding Protein Measurement," *Biotechnology Letters* 45, no. 11-12 (2023): 1431–1440, https://doi.org/10.1007/s10529-023-03425-4.

16. Z. B. Zadeh, S. M. Hosseini, J. Mohammadnejad, M. Tanhaei, and S. Ramakrishna, "Label-Free Detection of Cardiac Biomarkers: A Review on Microfluidic Electrochemical Biosensors," *ACS Applied Bio Materials* 6, no. 7 (2023): 2622–2635, https://doi.org/10.1021/acsabm.3c00257.

17. S. Liu, L. Wang, S. Liu, and Y. Zhao, "Donor–Derived Cell–Free DNA as a Diagnostic Biomarker for Acute Rejection in Heart Transplantation: A Systematic Review and Meta–Analysis," *Transplantation Reviews* 39, no. 2 (2025): 100916, https://doi.org/10.1016/j.trre.2025.100916.

18. F. Ranjbari, A. Nosrat, F. Fathi, and A. Mohammadzadeh, "Surface Plasmon Resonance Biosensors for Early Troponin Detection," *Clinica Chimica Acta* 558 (2024): 118670, https://doi.org/10.1016/j.cca.2024.118670.

19. M. A. Sacco, V. R. Aquila, S. Gualtieri, et al., "Quantification of Myocardial Biomarkers in Sudden Cardiac Deaths Using a Rapid Immunofluorescence Method for Simultaneous Biomarker Analysis," *Biomedicines* 13, no. 1 (2025): 193, https://doi.org/10.3390/biomedicines13010193.

20. R. M. Delgado, D. Núñez-Jurado, et al., "Smartphone-Enabled Point-of-Care Testing for Prehospital Stroke Diagnosis," *Prehospital Emergency Care* 12 (2024): 1–10.

21. A. I. Saviñon-Flores, F. Saviñon-Flores, G. Trejo, et al., "A Review of Cardiac Troponin I Detection by Surface Enhanced Raman Spectroscopy: Under the Spotlight of Point-of-Care Testing," *Frontiers in Chemistry* 10 (2022): 1017305, https://doi.org/10.3389/fchem.2022.1017305.

22. M. P. Ukpe and A. C. Ezeanuka, "Assessment of Accuracy, Clinical Validity, and Analytical Linearity in Point-of-Care Glucose Monitoring Devices for Diabetes Mellitus: A Systematic Review and Meta-analysis," *Clinical Biochemistry* 12 (2025): 110911, https://doi.org/10.1016/j.clinbiochem.2025.110911.

23. S. Odongo, B. K. Jin, H. T. T. Nguyen, M. Radwanska, and S. Magez, "A Nanobody/Monoclonal Antibody "Hybrid" Sandwich Technology Offers an Improved Immunoassay Strategy for Detection of African Trypanosome Infections," *PLOS Neglected Tropical Diseases* 18, no. 7 (2024): 0012294, https://doi.org/10.1371/journal.pntd.0012294.

24. Y. Zhang, Y. Chai, Z. Hu, et al., "Recent Progress on Rapid Lateral Flow Assay-Based Early Diagnosis of COVID-19," *Frontiers in Bioengineering and Biotechnology* 10 (2022): 866368, https://doi.org/10.3389/fbioe.2022.866368.

25. J. Baranwal, B. Barse, G. Gatto, G. Broncova, and A. Kumar, "Electrochemical Sensors and Their Applications: A Review," *Chemosensors* 10, no. 9 (2022): 363.

26. L. L. Ma, K. X. Xu, B. L. Xiao, et al., "An Electrochemical Sensor Based on NH2-MWCNTS-CMC and ZIF-67 Peroxidase-Like Nanocomposite for Sensitive Luteolin Detection," *Journal of the Iranian Chemical Society* 15, no. 15 (2024): 11319–11326.

27. H. A. Saputra, "Electrochemical Sensors: Basic Principles, Engineering, and State of the Art," *Monatshefte für Chemie Chemical Monthly* 154 (2023): 1083–1100.

28. E. Bou-Maroun, "Carbon Electrode Modified with Molecularly Imprinted Polymers for the Development of Electrochemical Sensor: Application to Pharmacy, Food Safety, Environmental Monitoring, and Biomedical Analysis," *Chemosensors* 11, no. 11 (2023): 548.

29. R. Liu, M. Zhao, X. Zhang, C. Zhang, B. Ren, and J. Ma, "Advances and Challenges in Molecularly Imprinted Electrochemical Sensors for Application in Environmental," *Biomedicine, and Food Safety, Critical Reviews in Analytical Chemistry* 6 (2025): 1–19.

30. J. Sun, Z. Wang, and J. Guan, "Single-Atom Nanozyme-based Electrochemical Sensors for Health and Food Safety Monitoring," *Food Chemistry* 425 (2023): 136518, https://doi.org/10.1016/j.foodchem.2023.136518.

31. M. B. Elamin, "Design of Novel Electrochemical Sensor Functionalized With Green Nanoparticles for Tetracycline Monitoring," *Polymers for Advanced Technologies* 35, no. 8 (2024): 6543, https://doi.org/10.1002/pat.6543.

32. N. Kumar, N. P. Shetti, S. Jagannath, and T. M. Aminabhavi, "Electrochemical Sensors for the Detection of SARS-CoV-2 Virus," *Chemical Engineering Journal* 430 (2021): 132966, https://doi.org/10.1016/j.cej.2021.132966.

33. S. Luo, Q. Wu, L. Wang, H. Qu, and L. Zheng, "Direct Detection of Doxorubicin in Whole Blood Using a Hydrogel-Protected Electrochemical Aptamer-Based Biosensor," *Talanta* 285 (2024): 127289, https://doi.org/10.1016/j.talanta.2024.127289.

34. A. Sarsenbayeva, S. Sadak, I. Kucuk, L. Kudreyeva, A. M. Bakytzhanovna, and B. Uslu, "Molybdenum-Based Electrochemical Sensors for Breast Cancer Biomarker Detection: Advances and Challenges," *Critical Reviews in Analytical Chemistry* 21 (2025): 1–21, https://doi.org/10.1080/10408347.2025.2487581.

35. Q. Yang, J. Pedreira-Rincón, L. Balerdi-Sarasola, et al., "An Aptamer-Based Electrochemical Sensor for the Quantification of the Malaria Biomarker Lactate Dehydrogenase," *Biosensors and Bioelectronics* 274 (2025): 117152, https://doi.org/10.1016/j.bios.2025.117152.

36. S. Zhong, L. Chen, X. Shi, G. Chen, D. Sun, and L. Zhang, "Recent Advances in Electrochemical Aptasensors for Detecting Cardiac Biomarkers: A Review," *Microchemical Journal* 193 (2023): 109063, https://doi.org/10.1016/j.microc.2023.109063.

37. R. Devaraj, A. K. Loganathan, and L. Krishnamoorthy, "Development of an Aptasensor for Highly Sensitive Detection of Cardiac Troponin I Using Cobalt–Nickel Metal-Organic Framework (CoNi-MOF)," *Heliyon* 10, no. 12 (2024): e33238, https://doi.org/10.1016/j.heliyon.2024.e33238.

38. X. Qin, D. Li, X. Qin, et al., "Electrochemical Detection of the Cardiac Biomarker Cardiac Troponin I," *View* 5, no. 5 (2024): 20240025, https://doi.org/10.1002/VIW.20240025.

39. E. C. Wilkirson, K. L. Singampalli, J. Li, et al., "Affinity-Based Electrochemical Sensors for Biomolecular Detection in Whole Blood," *Analytical and Bioanalytical Chemistry* 415, no. 18 (2023): 3983–4002, https://doi.org/10.1007/s00216-023-04627-5.

40. A. Stundl, R. Schulte, H. Lucht, et al., "Periprocedural Myocardial Injury Depends on Transcatheter Heart Valve Type But Does Not Predict Mortality in Patients After Transcatheter Aortic Valve Replacement," *JACC: Cardiovascular Interventions* 10, no. 15 (2017): 1550–1560.

41. K. Thygesen, J. S. Alpert, A. S. Jaffe, et al., "Fourth Universal Definition of Myocardial Infarction (2018)," *Journal of the American College of Cardiology* 72, no. 18 (2018): 2231–2264, https://doi.org/10.1016/j.jacc.2018.08.1038.

42. J. A. Bakker, A. D. Boymans, G. Dijkstra, and P. J. Lerk, "Rapid Determination of Serum Myoglobin With a Routine Chemistry Analyzer," *Clinical Chemistry* 39, no. 4 (1993): 653–658, https://doi.org/10.1093/clinchem/39.4.653.

Supporting Information

Additional supporting information can be found online in the Supporting Information section.

Supporting File 1: adhm71408-sup-0001-SuppMat.docx.

Supporting File 2: adhm71408-sup-0002-VideoS1.mp4.

Supporting File 3: adhm71408-sup-0003-VideoS2.mp4.

Supporting File 4: adhm71408-sup-0004-VideoS3.mp4.

Supporting File 5: adhm71408-sup-0005-VideoS4.mp4.